Modelling and engineering of stress based controlled oxidation effects for silicon nanostructures patterning

Xiang-Lei Han, Guilhem Larrieu, Christophe Krzeminski

Modelling and engineering of stress based controlled oxidation effects for silicon nanostructures patterning

Xiang-Lei Han

IEMN-UMR CNRS 8520, 59652 Villeneuve d'Ascq, France

Guilhem Larrieu

CNRS, LAAS, 7 avenue du colonel Roche, F-31400 Toulouse, France
Univ de Toulouse, LAAS, F-31400 Toulouse, France

E-mail: guilhem.larrieu@laas.fr

Christophe Krzeminski

IEMN-UMR CNRS 8520, Département ISEN, 41 Boulevard Vauban, 59046 France

E-mail: christophe.krzeminski@isen.fr

Abstract. Silicon nanostructure patterning with a tight geometry control is an important challenge at the bottom level. In that context, stress based controlled oxidation appears as an efficient tools for precise nanofabrication. Here, we investigate stress-retarded oxidation phenomenon in various silicon nanostructures (nanobeams, nanorings and nanowires) both at the experimental and theoretical levels. Different silicon nanostructures have been fabricated by a top-down approach. A complex dependence of the stress build-up with the nanoobjects dimension, shape and size have been demonstrated experimentally and physically explained by modelling. For the oxidation of a two dimensional nanostructure (nanobeam), a relative independence to size effects have been observed. On the other side, a radial stress increase with geometry downscaling of one dimensional nanostructure (nanowire) have been carefully emphasised. The study of the shape engineering by retarded oxidation effects for vertical silicon nanowires is finally discussed.

Submitted to: *Nanotechnology*

1. Introduction

Self-limited [1, 2, 3, 4, 5] or retarded [6] oxidation in silicon nanostructures is an interesting technological tool in order to manipulate the geometrical (the shape [7], the size [8], the distribution [9]) or the physical properties [1, 10, 11] of silicon nano-objects. Several applications have been foreseen using this effect such as a nano-field effect transistor [12], nanoflash memory [13, 14, 15]. However, the physical mechanisms underlying remain poorly understood at the fundamental level and more knowledge is needed. The computer simulation of such a processing is an identified issue. Atomistic simulations are only able to describe the very first stage of the oxidation process [16, 17]. Large concerns about the stress levels predicted at the atomistic scale of the Si/SiO_2 interface have been reported [18]. On the other hand, macroscopic simulations [19] fail to explain these retarded or self-limited effects and cannot be used to predict the resulting shape of the oxidised nanostructures [20]. This is a large concern for silicon based nanotechnology which should be addressed.

In this work, we present a large experimental and modelling study of the stress-retarded oxidation effects and their influence in the nanostructure shape engineering. Here, the seminal work of Kao *et al.* [21, 22] is revisited in various aspects, pointing out the size effects in the oxidation of silicon nanostructures at the nanoscale level. First, the orientation effects on simple planar bulk oxidation have been carefully investigated in the experimental range. The influence of the surface shape (concave/convex) of the nanoobject has been observed and quantified by the modelling of the oxidation kinetics. For the nanobeam structure, the Finite Element Method (FEM) has been able to explain the general shape of the oxidised structure but also the absence of retarded effect with the scaling of the nanostructure width. Finally, size dependent self-limited oxidation effects in silicon nanowires is reported and evaluated. Experimentally, the improvement of the high anisotropic character with self-limited oxidation effects is demonstrated. The engineering of the aspect ratio and the shape of the silicon nanowires with oxidation conditions is analysed. The simulation shows that the initial regime where both reaction and diffusion limited regime coexist should be preferred in order to increase the final anisotropy and improve the vertical profile.

2. Experiments

In these experiments, various silicon nanostructure geometries (vertical nanobeams, nanorings, and nanowires) have been fabricated with a high control thanks to a top-down approach [23]. As shown in figure 1.A1-3, nanomasks patterned by electron-beam lithography using a negative tone electron-beam resist (Hydrogen Silesquioxane) HSQ have been fabricated. A very high contrast has been achieved using an important acceleration voltage (100kV), a very small beam size at a current of 100 pA and a concentrated developer, 25 % Tetramethylammonium. The different type of silicon

structures obtained after the mask transfer by chlorine based plasma etching followed by the stripping of the HSQ resist using 10% HF are shown in figures 1.B1-3). Finally, wet oxidation have been carried out in a horizontal furnace (TEMPRESS) at 850°C under a mixed flow of 1.5L/min of O_2 and 2.5L/min of H_2. Figure 1.C1-3) shows the resulting nanoobjects after the oxidation step and oxide stripping by the wet etching step. Compared to other methods like AFM nanolithography based local oxidation [24] where ultimate planar silicon nanowires have been fabricated [25, 26], the oxidation nanolithography process adopted here is observed to be a complementary approach to pattern silicon surface and to control the vertical shape of various Si nanostructures.
The various nanostructures have been carefully characterised after the oxidation process. All the different images have been acquired with a high resolution Scanning Electron Microscopy, SEM, (ZEISS ULTRA 55 system at 10kV, and WD $\sim$ 4 mm). In the case of SiNWs, the diameters of oxidised SiNWs (d_{ox}) and after the striping of SiO_2 layer (d_{Si}) have been measured at the NW mid-height by tilted view. The grown SiO_2 layer thickness (t_{ox}) is estimated by the difference between d_{Si} and t_{ox}. In the case of silicon nanorings, the SiO_2 layer thickness for inner diameters has been evaluated using top view images. Finally, in the case of the nanobeams, the oxide thickness has been quantified with cross section view.

3. Silicon oxidation modelling

Oxidation modelling matching as closely as possible the experimental work has been undertaken. A large debate exists on the nature of the atomic transport and the reaction process during the growth of silicon dioxide [27]. Classically, the thermal planar silicon oxidation kinetics are modelled by the seminal Deal and Grove approach [28]. The physical picture mostly accepted in the literature for silicon oxidation process is that the reaction is driven i) by the transport from the ambient to the top surface ii) by the diffusion of the oxidant species across the amorphous oxide layer and finally iii) by the reaction with silicon atoms. In the case of wet oxidation, the diffusive species is an interstitial H_2O molecule which is incorporated in the silica network:

$$H_2O + Si - O - Si \rightarrow 2Si - OH \tag{1}$$

and diffuses quickly within the SiO_2 layer [29]. The incorporation of hydroxyl content ([OH]) has a major influence on the mechanical parameters (viscosity) of the silica network. The reaction scheme at the silicon interface with the silicon bonds is then described by [30]:

$$H_2O(SiO_2) + Si - Si \rightarrow Si - O - Si + H_2(SiO_2) \tag{2}$$

It has been shown that for planar bulk silicon oxidation (see figure 2.a), the oxide thickness x generated by equation (2) follows a linear-parabolic kinetics as function of the annealing time [28]:

$$\frac{x^2}{(B)} + \frac{x}{(B/A)} = t + \tau \tag{3}$$

where (B/A) is the linear rate constant and (B) the parabolic rate for silicon bulk oxidation. The linear rate constant depends linearly on the reaction rate at the Si/SiO_2 interface whereas the parabolic term is linked to the oxidant species diffusivity in the oxide. However, this model must be extended by introducing stress effects for non-planar configuration. Despite several efforts [31], the modelling of 3D silicon oxidation remains a complex issue. First, the non-linear dependences on stress of several key parameters (reaction rate, oxidant diffusivity, viscosity) is difficult to handle rigorously [32, 33]. Next, the description of the moving boundaries at the Si/SiO_2 interface using FEM [34, 35] is still problematic. Performing a physical and complete 3D simulation of silicon oxidation on such nanometric structures remains challenging. To overcome such issues, the following pragmatic approach has been undertaken. First, a reliable two dimensional viscoelastic oxidation model present in most TCAD process simulators has been applied to study the nanobeam structure (2D structure). Moreover, an analytic oxidation model which enables the description of silicon cylinder oxidation effects [33] has been implemented. Despite some limitations, these two approaches have been observed to be fully complementary in order to support the experimental studies.

3.1. 2D Process simulation

Finite elements based process simulations have been undertaken in this study in order to improve the understanding of the dimensional oxidation effects observed experimentally at the nanoscale level in the nanobeam structure as shown in figure 2.(b). Process modelling [36] using finite elements based simulators (TSUPREM-4) has been used. A large set of nanobeam structures matching all the experimental features details provided by SEM characterisation have been simulated [37]. As pointed out in a recent study [20], most of the process simulator fails to describe the nanostructure shape resulting from the oxidation process. In order to improve the predictivity of the oxide growth rate in the (110) and (111) orientation, the linear rate has been re-calibrated as discussed in sec 4.1. At a (x,y) position of the Si/SiO_2 interface, the oxidation velocity is given by the following equation (4) [38] :

$$v(x,y) = \frac{(\alpha - 1)}{N} k_{Si}(x,y) C(x,y) \vec{\eta}(x,y) \tag{4}$$

where α is the volume expansion factor of silicon to oxide conversion ($\alpha = 0.44$), $\vec{\eta}(x,y)$ is the normal direction at the Si/SiO_2 interface, N is the number of oxidant molecules incorporated into a unit volume of the oxide. In this formalism, the oxidation rate is directly linked to the linear rate constant (B/A) of the Deal and Grove approach by introducing C^* the oxidant solubility in the silicon dioxide :

$$k_{Si} = (B/A)\frac{N}{C^*} \tag{5}$$

As observed by Kao *et al.* [21, 22] for the wet oxidation of a micrometer cylinder, the influence of a normal stress σ component at the Si/SiO_2 interface exponentially

reduces the oxidation rate with :

$$\begin{cases} (B/A)^{\sigma} = (B/A)\exp\left(\dfrac{-\sigma V_k}{k_B T}\right) & \text{for } \sigma < 0 \\ (B/A)^{\sigma} = (B/A) & \text{for } \sigma \geq 0 \end{cases} \tag{6}$$

where k_B is the Boltzmann constant and T is the oxidation temperature in Kelvin, V_k corresponds to an activation volume.

$$D = B_0(T) \cdot \frac{N}{2C^*} \tag{7}$$

The oxidation rate $v(x, y)$ is also driven by the oxidant concentration at the interface which itself is governed by the oxidation diffusivity in the oxide. In this case, the stress influence is described by the hydrostatic pressure $P = -0.5 \cdot (\sigma_{xx} + \sigma_{yy})$ located in the oxide :

$$\begin{cases} D^P = D\exp\left(\dfrac{-PV_d}{k_B T}\right) & \text{for } P > 0 \\ D^P = D & \text{for } P \leq 0 \end{cases} \tag{8}$$

This equation can be viewed as a way to incorporate the influence of density change on the oxidation diffusivity in the oxide ‡. Therefore, oxidation stress dependent effects should be taken into account and the oxidation is either limited by the reaction rate or/and by the oxidant supply through the reduced oxidation diffusion.

For two dimensional simulations, stress dependent oxidation parameters are being used but the main issue is probably to accurately describe the mechanical behaviour of the Si/SiO_2 system and, more specifically, the mechanical relaxation phenomena involved during the reaction in the SiO_2. A viscoelastic approach is commonly used in order to model the plastic strain relaxation in the oxide [19] governed by the viscosity η :

$$\eta(\tau) = \eta_0 \frac{(\tau/\sigma_c)}{\sinh(\tau/\sigma_c)} \tag{9}$$

where τ is the shear stress, σ_c is the critical shear strain and η_0 is the zero stress state viscosity. It should be underlined that the oxidising ambient has a major influence on the zero stress oxide viscosity and, as a consequence, on the stress generated during oxidation. The incorporation of hydroxyl content in SiO_2, described by the equation (1), is of particular importance since wet oxidation is characterised by a high zero stress state viscosity [29, 40]. One of the main difficulties resides in the introduction of the stress dependence on viscosity, which generates large numerical instability [41]. However, neglect of plasticity relaxation, described in (eq. 9), often leads to assume very low stress state viscosity in order to achieve reasonable stress levels [42]. One consequence is the

‡ Initially the model assumed was that the diffusivity depends on the volumetric strain ϵ_v with $D = D_0 \exp(a\epsilon_v)$. This volumetric strain depends linearly on the pressure if a slow variation of the applied pressure is assumed [39]

underestimation of the stress levels for the nanoobject subject to much moderate stress as described in section 4.3 for the case of nanobeam oxidation. In the case of these 2D simulations, the variation of the shear stress and the viscosity are not self-consistently solved, which limits the validity domain of the simulation to relatively low stress levels mainly below σ_c.

3.2. Plastic analytic extension for cylindric nanoobjects

The implementation of the previous approach from 2D to 3D nanostructures is not straightforward and a rigorous extension to describe the oxidation of cylinder shape nanoobjects (see Figure 2) is necessary. In our experimental conditions, a large deformation rate is induced by the oxidation of the nanoobjects and requires that plastic relaxation effect are properly introduced, as discussed in a previous publication [43]. The oxidation velocity at the Si/SiO_2 interface can be described by equation (10):

$$v(a) = \frac{(\alpha - 1)}{N} \frac{C^*}{\frac{1}{k^{\sigma}_{Si}} \pm \frac{a}{D^{P}_{SiO_2}} \log(\frac{b}{a})}. \tag{10}$$

$$\tau(r) = \frac{2\eta a \nu}{r^2} \tag{11}$$

It should be emphasised that the shear stress dependent viscosity (eq. 9), the oxidation growth rate (eq. 10) and the shear stress (eq. 11) are coupled with each others. The fact that all these equations must be self-consistently solved is often overlooked or not exactly taken into account. Following Rafferty *et al.* [33], the shear (τ), radial (σ_r) and tangential (σ_θ) stress field component in the silicon dioxide of a cylinder structure (see 1.(b) can be expressed as :

$$\begin{cases} \tau(r) = \sigma_c \sinh^{-1}\left(\frac{2R^2}{r^2}\right) \\ \sigma_r(r) = \pm\frac{1}{2}\sigma_c\left[\left(\ln\frac{R^2}{b^2}\right)^2 - \left(\ln\frac{R^2}{r^2}\right)^2\right] \\ \sigma_\theta(r) = \sigma_r(r) - 2\tau(r) \end{cases} \tag{12}$$

with the reduced parameter $R = \sqrt{\frac{4\eta_0 a v}{\sigma_c}}$. Compared to a standard viscous approach [22] with a constant viscosity, the radial stress build-up has a logarithmic dependence on the curvature radius, leading to great opportunities to investigate the oxidation of cylinder shape nanostructures and the impact of the nanostructures geometry on the oxidation behaviour.

4. Results and discussion

The main challenges associated with the shape ratio engineering by oxidation at the nanoscale level of silicon nanostructures are the complex interplay between several physical effects addressed in the next section by incremental difficulty. First, orientation

effects are estimated on bulk planar silicon oxidation layer. Next, the concave/convex character is quantified by oxidising large silicon nanostructures. In these two simple cases, it will be shown that some standard key TCAD parameters are not suitable in order to simulate these basic experiments. Next, the oxidation study of silicon nanobeams is reported in large details. Different effects have been observed resulting from the complex stress field generated by a concave and convex shape and its independence with the dimension variation. Finally, size effects resulting in silicon nanowires have been investigated in details.

4.1. Orientation effects and planar oxidation

The silicon substrate orientation is known to influence significantly the thermal oxidation rate [44]. However, at the nanoscale level, it is really difficult to separate the influence of crystalline orientation from the other contributions like geometry or stress effects. In order to rule out the influence of orientation effects, planar silicon bulk wet oxidation experiments have been conducted on three different orientations (100), (110) and (111). Figure 3.(a) compares these different experimental oxidation kinetics (red dots) with the standard analytic Deal and Grove kinetics using conventional TCAD parameters (red dashed lines). A quasi-linear behaviour is observed for the various kinetics whatever the crystalline orientation, indicating that the oxidation process for planar bulk is clearly reaction rate limited. The impact of surface orientation effect is evidenced with the following order for the oxidation rate : $v(110) > v(111) > v(100)$ as function of the substrate orientation. A similar experimental study at a lowest temperature (785°C) has been performed by Ngau *et al.* [45] (experimental data are reported in figure 3.(a)). This initial anomalous enhancement of the $v(110)$ oxide rate for the oxidation time considered have also been observed in figure 3.(a). However, the curious crossover between $v(110)$ and $v(111)$ by Ngau *et al.* occurred at much longer oxidation time.

From a modelling point of view, the influence of crystalline orientation effects on bulk oxidation rates has been related to the reaction rate which is directly dependent on the number of silicon bonds available at the Si/SiO_2 interface [30]. The oxidation kinetics are well described only for the (100) case whereas the enhancement observed for (110) is strongly underestimated, especially in the short time regime. The physical mechanisms responsible for these oxidation effects remain unclear. The variation of intrinsic stress among substrate orientation [46] is a plausible explanation [45] but the possible influence of the density of atomic sites available at the interface cannot be ruled out [30]. Empirically, a rough description is performed since it has been assumed that the linear rate (B/A) is being increased by a linear factor for (110) and (111). These different prefactors associated with the various crystalline planes have been re-calibrated in order to minimise the normalised mean square error between the experimental and theoretical oxide thickness summarised in Table 1. The linear rate for these two specific

orientations is given by :

$$\begin{cases} \left(\frac{B}{A}\right)_{(110)} = 2.25\left(\frac{B}{A}\right)_{(100)} \\ \left(\frac{B}{A}\right)_{(111)} = 1.57\left(\frac{B}{A}\right)_{(100)} \end{cases} \quad (13)$$

The influence of silicon orientation on the linear rate and the complex behaviour of the growth rate preserves a part of its mystery. The fact that the planar oxidation is not a pure stress free reference [46, 47, 48] as described by the planar Deal and Grove model could be a plausible explanation. The pragmatic solution adopted by re-calibrating the linear rate on bulk oxidation experiments gives us a reasonable solution to describe empirically the orientation effects. Figure 3.(b) shows that a nice agreement can be reached with a mean square error less than 1 nm provided these two standard parameters used in TCAD tools are properly re-calibrated.

4.2. Concave/convex oxidation effects and cylindric nanostructures

Finally, the geometry effects (concave/convex shape) have been investigated on large nanostructures in order to limit the influence of dimension effects. In many previous works [19, 21, 22, 49, 50, 51], the study of micrometer shaped silicon surfaces is mostly related to the development of isolation structures for silicon transistors such as local oxidation (LOCOS) [52] and later shallow trench isolation process (STI). The impossibility to describe these complex retarded oxidized surfaces with the standard Deal and Grove model [50] have involved a general introduction of stress effects into the kinetic parameters as shown in (eq. 6,8). Despite the progressive refinement of the generalised stress dependent Deal and Grove model [19], our work highlights the limits in terms of modelling in TCAD tools.

The experimental variation observed for the oxide thickness with concave/convex nanostructures has been characterised in figure 4. First, the presence of retarded oxidation effects in these nanostructures is easily illustrated when compared to the (110) bulk oxidation kinetics. The oxidation rate should be observed on the lateral side of the cylindric nanostructure. Considering the same oxidation range, the planar case shows linear oxidation kinetics whereas parabolic evolutions are in the nanostructures oxidation kinetics. Concave/convex geometries exhibit different behaviours during the oxidation process, in agreement with the seminal work of Kao *et al.* [21] on micrometer scale. The oxidation of 70 nm wide convex or concave nanostructures shows that the retarded oxidation effect is exacerbated in the concave case. At least a factor between 1.8 and 2 can be observed in terms of oxide growth for the 70 nm width between oxide thickness grown in concave and convex nanostructures.

Oxidation kinetics have been simulated using the plastic model described in section 3.2 and the standard parameters (except orientation effects) used in TCAD tools described in section 3.1. As presented in figure 4.(a), the retarded oxidation effects for convex nanostructures are nicely described. As shown previously [43], the main effect predicted by simulation is a significant radial stress build-up during oxidation which decreases the reaction rate. On the other hand, the retarded oxidation effects in the concave case are strongly overestimated by the model. For the smallest concave nanostructure, a completely limited oxidation regime is predicted which is not experimentally the case. It could be noticed that the largest discrepancy is observed for the largest concave nanostructure where the impact of the stress should be much lower. The main factor of the divergence between experiments and simulation is identified as an overestimation of the hydrostatic pressure effect on the oxygen diffusivity :

$$D^P = D \exp\left(\frac{-PV_d}{k_B T}\right). \tag{14}$$

The activation volume of diffusivity takes the influence of the hydrostatic pressure into account. Parameter (V_d=75 Å^3) is used as a reference in several studies [19, 51] and corresponds to the standard parametrisation used in several commercial process simulators. As shown in figure 4.(a), this parameter tends to overestimate the diffusion oxidation limited effects. In contrast, figure 4.(b) illustrates that both retarded oxidation effects in concave or convex structures could be properly described if the activation volume is reduced to 45 Å^3.

4.3. Nanobeam oxidation effects

Compared to the previous planar bulk and the large cylindrical nanostructure, nanobeams exhibit a more complex geometry with a two dimensional profile. As a consequence, the variation of oxide thickness as a function of the nanobeam geometry (height and width) shows unexpected size behaviour.

Experimentally, the oxide thickness measured at the half of the beam height has been reported in figure 5.(a) according to the beam width and height. Two main results are observed : i) the oxide thickness is constant for a defined beam height and ii) the oxide thickness for the 2 beam heights (110 nm and 240 nm) are different. In other words, the experimental oxide growth rate is independent of the nanobeam width and is faster in higher structures. For the shortest oxidation duration (10 min.), the kinetics for to different heights (110 and 240 nm) are relatively similar to the [110] bulk oxidation kinetics. The situation is slightly different for a longer oxidation (20 min) case where the kinetics is lower for the smaller nanobeam heights. It should be noticed that, i) no self-limited oxidation effects occurred with the silicon nanobeams and ii) for the narrowest nanobeams (below 40 nm), a complete consumption of the silicon is reached and noticed by an open symbol in figure 5.(a). SEM cross sections of a 70 nm width nanobeam after a wet oxidation step at 850°C for the two different oxidation times and

heights provide more details about the oxidation mechanism. A classical non-uniform profile is observed in the different regions of the structure. Firstly, from a geometrical point of view, the top corners and bottom corners of the nanobeam exhibit a convex and concave structure respectively. The oxide growth associated to these configurations, as discussed in the previous section, is enhanced in the top corner and reduced in the bottom corner. Secondly, the oxide thickness is thinner in the (100) direction due to a different oxidation rate with the silicon crystalline direction. Thirdly, the oxide growth is non uniform along the sidewall of the beam with the quickest oxidation in the middle section of the structure. The ratio of oxide thicknesses measured at the middle and at the top of the nanobeam is estimated at 2.2 and 2 respectively for 110 nm height in figure 5.(a) and (b) whereas for 240 nm height it is evaluated at 2.3 and 2.5 in figure 5.(c). It is worth noting in figure 5.(c) that the higher structure (240 nm) is less affected by the non-uniform oxide growth (110 nm).

Two dimensional finite elements based simulations described in section 3.1 have been able to provide sufficient physical insight in order to explain these various effects. A sharp comparison between the experimental profile and FEM modelling is illustrated in figure 6. The experimental nanobeam structures after 10 min. (a) (resp. 20 min (c)) of wet oxidation and the corresponding results of process simulation (b) (resp. (d)) are presented. An overall nice agreement between the experiment and the shape predicted is obtained. Orientation effects take place effectively, as shown by the comparison between the limited oxide thickness on the [100] far from the nanobeam and the sidewall oxide thickness. These trends are correctly described thanks to the previous calibration of orientation effects. Strong retarded effects are observed in the concave corner at the bottom of the nanobeam and related to the large pressure hydrostatic level (higher than 500 MPa) predicted by FEM modelling. As shown by figure 6.(b), the lateral normal stress distribution (σ_{xx}) is non-uniformly distributed along the vertical direction of the nanobeam. A longer oxidation time tends to enhance this non-uniformity which can explain the formation of a fully separated nanowire/nanotriangular shape surrounded by SiO_2 by only stress effects [13, 14, 15]. Again the predicted shape in figure 6.d) is particularly relevant as regards the structure complexity. The oxidation of lateral 2D shape of the nanobeams, the presence of different crystalline orientations and concave/convex shape induced a stress field which is responsible for the different effects observed.

Based on FEM modelling, the oxide thickness obtained for several nanobeam widths and heights have been simulated (Figure 7.(a)). The two experimental trends are also visible with the simulation i) no retarded oxidation dependence with the nanobeam width ii) limited oxidation effects increase with decreasing nanobeam height. The lateral stress build-up at mid-height during oxidation in figure 7.(b) demonstrates a faster compressive stress build-up for the shortest structure. This compressive stress which is the major reason for reaction rate limited effects enlightens the experimental difference observed in figure 5.(a). The most interesting result is the lateral stress variation with

the nanobeam width given by figure 7.(c). When the silicon core is not fully oxidised, the variation are relatively modest and a mean level of lateral stress can be defined as function of nanobeam widths. This result also easily explains the independence of the oxidation behaviour with nanobeam widths.

4.4. Limited oxidation effects in silicon nanowires

The direct comparison of the oxidation behaviour between a silicon nanobeam (width=53 nm) and nanowire (diameter=43 nm) in figure 8 emphasises the importance of the dimensional aspect. While the two dimensional oxidised profile of the nanobeam presents a characteristic non homogeneous anisotropic profile as explained in section 4.3, the one dimensional nanowire has a very uniform shape. Despite the initial presence of a convex shape at the bottom, the nanowire does not present a necklace shape (inset of figure 8.(b) after oxidation which could indicate that a widespread compressive stress take place around the nanowire. A common feature is the limited oxide growth observed at the bottom end of the nanowire where the concave shape also influences the growth by diffusion limited oxidation effects. However the effect seems to be less predominant in the nanowire. The technical interest of the resulting silicon profile will be discussed in section 5.

Self-limited or retarded effects during the oxidation of nanowire has been characterised in details. Figure 9.(a) and .(b) present respectively the evolution of the SiNW diameter and the oxide thickness as a function of the oxidation time. The experimental dots give the remaining silicon diameter after oxidation and oxide stripping while the dashed lines presents the simulated evolution obtained with the one dimensional model discussed in section 3.2. Despite the rough approximation, since the experimental sidewalls of the nanowire are not strictly vertical, the one dimensional model is effective to describe the oxidation kinetics. A slowdown of the oxidation kinetics has been identified. Compared to the nanobeam oxidation, limited oxidation effects have been observed to be highly dependent on the nanowire diameters. The evolution of the oxidation rate for different SiNWs diameters shown in figure 9.(c) confirms these conclusions. While initially being close to 3 nm/min., the rate decreases very quickly down to 1 nm/min. This effect can be explained thanks to the compressive stress build-up provided in the inset of figure 9.(c) which tends to decrease the linear oxidation rate as described in (eq. 6). The normal radial stress at the silicon interface of the nanowire slows down the oxidation rate by making the reaction of Si to SiO_2 less energetically favourable. This radial compressive stress build-up is much more effective here than in the nanobeam case due to its more confined structure of the SiNWs. Figure 9.(d) describes the evolution of the other kinetic parameter in the Deal and Grove framework, the parabolic rate. The initial hydrostatic pressure at the Si/SiO_2 interface being tensile, no diffusion limited oxidation effect takes place. A significant oxide growth is necessary in order to change the longitudinal stress from tensile to compressive and to reach a widespread compres-

sive hydrostatic pressure. The appearance of diffusion limited oxidation can explain the quasi self-limited oxidation effects for the silicon nanowire with 40 min. of wet oxidation.

5. Silicon nanowires thinning and aspect ratio engineering

Vertical silicon nanowire arrays are a promising architecture for the implementation of ultimate logic devices [53] or nanosensors and are routinely fabricated either by bottom-up [54] or top-down approaches [23]. One of the key issues for all sub-20 nm devices is the variability concern generated since large fluctuations of geometrical properties (width, length, shape, gate oxide thickness) can be observed during the manufacturing of a large number of these nanoobjects. A large impact on various electrical properties (threshold voltage, geometry dependent capacitance) are expected [55]. Here, one of the most difficult geometric parameters to control is the sidewall anisotropy ratio since near vertical sidewall profile should be achieved with a small variability for the manufacturing of vertical SiNWs based nanodevices.

Self-retarded silicon oxidation effects have been used to overcome the various technological concerns since a better control of the nanowire radius and shape could be achieved with the remaining silicon core. Figure 10.(a) details the experimental evolution of the anisotropic character with the silicon diameter. An increase in the anisotropic character is effectively observed for each nanowire, the effect for the thinnest nanowire being more effective at least for the short oxidation time. After a wet oxidation of 20 min. followed by an etching of the oxide layer, the anisotropy profile of SiNWs has been improved from 92% up to 99% with the reduction of the SiNWs diameter (around 14 nm) for the thinnest nanowire (initially 33 nm). Insets (b) to (d) of figure 10 show that the sidewall anisotropy of silicon nanowires has been effectively increased during oxidation.

The modelling of the aspect ratio engineering is a complex task as a three dimensional simulation of oxidation should be rigorously undertaken, as discussed in section 3.2. A first approximation has been undertaken by considering that the real nanowire is made of several anisotropic nanowires of different diameters matching the initial experimental aspect ratio. The theoretical improvement of the anisotropic character is given in figure 11.(a). The model predicts effectively an increase in the aspect ratio from 92 % to up 94 % for 133 nm NWs or 96% for the thinnest 43 nm NWs. In agreement with the experimental results, the aspect ratio increases for short oxidation times (below 20 min) and saturate with the dominance of diffusion limited oxidation effects. It could be noticed that the model underestimates the aspect ratio improvement compared to the experimental value since much more vertical sidewalls have been obtained experimentally. Despite these limitations, some interesting conclusions for further experimental work can be extracted. The importance to favour the reaction rate limited regime for the sharpening of the aspect ratio is highlighted in figure 11.(b). The following scenario has been investigated by simulation. A 43 nm diameter silicon nanowire free of stress

with a surrounding oxide of the same thickness has been considered. The presence of this large oxide prevents an initial tensile hydrostatic pressure described in figure 9.(c) and drives the appearance of retarded diffusion effects at the beginning of the oxidation step. It can be observed that effectively, the aspect ratio engineering would be less effective compared to the standard case where initially only reaction rate limited oxidation effects take place. This result would be of interest since oxidation/etching and stress release could be foreseen in order to maximise the shape ratio engineering. Finally, the impact of the initial anisotropic character has also been studied by simulation. The results, given by figure 11.(c), show that the use of retarded oxidation effect would be clearly beneficial when the anisotropic profile of vertical SiNWs decreases.

6. Conclusion

The modelling of retarded oxidation in various silicon nanostructures have been investigated in depth based on a pragmatic approach that coupled 2D TCAD tools and a one dimensional plastic model. Limits in the simulation and the parametrisation of orientation effects and concave shape nanobjects have been emphasised. Large difference in oxidation scheme for multidimensional nanostructures have been successfully explained by modelling and in particular by the estimation of the radial stress build-up. The engineering of the nanowire sharpening and the aspect ratio through retarded oxidation effects have been demonstrated. The different simulations confirm some experimental trends observed. The model also indicates that the initial regime where reaction rate and diffusion limited effects due to the compressive radial stress build-up is more favourable for the aspect ratio engineering of SiNWs.

Acknowledgments

This work was supported by the European Commission through the NANOSIL Network of Excellence (FP7-IST-216171) and the RTB platform (French national nanofabrication network, RENATECH). The financial support of ANR QUASANOVA is also acknowledged.

References

[1] R. Okada and S. Iijima. Oxidation property of silicon small particles. *Applied Physics Letters*, 58(15):1662–1663, 1991.

[2] H. I. Liu, D. K. Biegelsen, N. M. Johnson, F. A. Ponce, and R. F. W. Pease. Self-limiting oxidation of si nanowires. In *Proceedings of the 16th international symposium on electron, ion, and photon beams*, volume 11, pages 2532–2537. AVS, 1993.

[3] H. Cui, C. X. Wang, and G. W. Yang. Origin of self-limiting oxidation of si nanowires. *Nano Letters*, 8(9):2731–2737, 2008. PMID: 18680350.

[4] H. I. Liu, D. K. Biegelsen, F. A. Ponce, N. M. Johnson, and R. F. W. Pease. Self-limiting oxidation for fabricating sub-5 nm silicon nanowires. *Applied Physics Letters*, 64(11):1383–1385, 1994.

[5] H. Heidemeyer, C. Single, F. Zhou, F. E. Prins, D. P. Kern, and E. Plies. Self-limiting and pattern dependent oxidation of silicon dots fabricated on silicon-on-insulator material. *Journal of Applied Physics*, 87(9):4580–4585, 2000.

[6] C. C. Büttner and M. Zacharias. Retarded oxidation of si nanowires. *Applied Physics Letters*, 89(26):263106, 2006.

[7] G. Pennelli. Top down fabrication of long silicon nanowire devices by means of lateral oxidation. *Microelectronic Engineering*, 86(11):2139 – 2143, 2009.

[8] Y. Chen and Y. Chen. Modeling silicon dots fabrication using self-limiting oxidation. *Microelectronic Engineering*, 57-58:897 – 901, 2001. Micro- and Nano-Engineering 2000.

[9] H. Coffin, C. Bonafos, S. Schamm, N. Cherkashin, G. Ben Assayag, A. Claverie, M. Respaud, P. Dimitrakis, and P. Normand. Oxidation of si nanocrystals fabricated by ultralow-energy ion implantation in thin sio[sub 2] layers. *Journal of Applied Physics*, 99(4):044302, 2006.

[10] G. Stan, S. Krylyuk, A. V. Davydov, and R. F. Cook. Compressive stress effect on the radial elastic modulus of oxidized si nanowires. *Nano Letters*, 10(6):2031–2037, 2010. PMID: 20433162.

[11] Y.-M. Niquet, C. Delerue, and C. Krzeminski. Effects of strain on the carrier mobility in silicon nanowires. *Nano Letters*, 12:3545, 2012.

[12] K. Trivedi, H. Yuk, H. C. F., M. J. Kim, and W. Hu. Quantum confinement induced performance enhancement in sub-5-nm lithographic si nanowire transistors. *Nano Letters*, 11(4):1412–1417, 2011.

[13] X. Tang, N. Reckinger, V. Bayot, C. Krzeminski, E. Dubois, A. Villaret, and D.-C. Bensahel. Fabrication and room-temperature single-charging behavior of self-aligned single-dot memory devices. *Nanotechnology, IEEE Transactions on*, 5(6):649 –656, nov. 2006.

[14] X. Tang, C. Krzeminski, A. Lecavelier des Etangs-Levallois, Z. Chen, E. Dubois, E. Kasper, A. Karmous, N. Reckinger, D. Flandre, L. A. Francis, J.-P. Colinge, and J.-P. Raskin. Energy-band engineering for improved charge retention in fully self-aligned double floating-gate single-electron memories. *NanoLetters*, 11:4520–4526, 2011.

[15] C. Krzeminski, X. Tang, N. Reckinger, V. Bayot, and E. Dubois. Process optimization and downscaling of a single-electron single dot memory. *Nanotechnology, IEEE Transactions on*, 8(6):737 –748, nov. 2009.

[16] J. Dalla Torre, J.-L. Bocquet, Y. Limoge, J.-P. Crocombette, E. Adam, G. Martin, T. Baron, P. Rivallin, and P. Mur. Study of self-limiting oxidation of silicon nanoclusters by atomistic simulations. *Journal of Applied Physics*, 92(2):1084–1094, 2002.

[17] B.-H. Kim, M. A. Pamungkas, M. Park, G. Kim, K.-R. Lee, and Y.-C. Chung. Stress evolution during the oxidation of silicon nanowires in the sub-10 nm diameter regime. *Applied Physics Letters*, 99(14):143115, 2011.

[18] T. Watanabe. Dynamic bond-order force field. *Journal of Computational Electronics*, 10:2–20, 2011.

[19] V. Senez, D. Collard, B. Baccus, and J. Lebailly. Analysis and application of a viscoelastic model for silicon oxidation. *J. Appl. Phys.*, 76:3285, 1994.

[20] F.-J. Ma, S. C. Rustagi, G. S. Samudra, H. Zhao, N. Singh, G.-Q. Lo, and D.-L. Kwong. Modeling of stress-retarded thermal oxidation of nonplanar silicon structures for realization of nanoscale devices. *IEEE Electron Device Letters*, 31(7):719, 2010.

[21] D.-B. Kao, J.P. McVittie, W.D. Nix, and K.C. Saraswat. Two-dimensional thermal oxidation of silicon;i. experiments. *Electron Devices, IEEE Transactions on*, 34(5):1008 – 1017, may 1987.

[22] D.-B. Kao, J.P. McVittie, W.D. Nix, and K.C. Saraswat. Two-dimensional thermal oxidation of silicon. ii. modeling stress effects in wet oxides. *Electron Devices, IEEE Transactions on*, 35(1):25 –37, jan 1988.

[23] X.-L. Han, G. Larrieu, P.-F. Fazzini, and E. Dubois. Realization of ultra dense arrays of vertical silicon nanowires with defect free surface and perfect anisotropy using a top-down approach. *Microelectronic Engineering*, 88(8):2622 – 2624, 2011.

[24] Ricardo Garcia, Montserrat Calleja, and Heinrich Rohrer. Patterning of silicon surfaces with

noncontact atomic force microscopy: Field-induced formation of nanometer-size water bridges. *Journal of Applied Physics*, 86(4):1898–1903, 1999.

[25] Ricardo Garcia, Ramses V. Martinez, and Javier Martinez. Nano-chemistry and scanning probe nanolithographies. *Chem. Soc. Rev.*, 35:29–38, 2006.

[26] J. Martinez, R. V. Martnez, and R. Garcia. Silicon nanowire transistors with a channel width of 4 nm fabricated by atomic force microscope nanolithography. *Nano Letters*, 8(11):3636–3639, 2008. PMID: 18826289.

[27] I. J. R. Baumvol. Atomic transport during growth of ultrathin dielectrics on silicon. *Surface Science Reports*, 36(1-8):1 – 166, 1999.

[28] B. E. Deal and A. S. Grove. General relationship for the thermal oxidation of silicon. *Journal of Applied Physics*, 36(12):3770–3778, 1965.

[29] S. M. Hu. Effect of process parameters on stress development in two-dimensional oxidation. *Journal of Applied Physics*, 64(1):323–330, 1988.

[30] J. R. Ligenza. Effect of crystal orientation on oxidation rates of silicon in high pressure steam. *The Journal of Physical Chemistry*, 65(11):2011–2014, 1961.

[31] T. Hoffmann, K. F. Dombrowski, and V. Senez. On 2d/3d numerical oxidation modeling: Calibration and investigation of silicon crystal orientation effect on stresses in shallow trench isolations. *Technical Proceedings of the 2000 International Conference on Modeling and Simulation of Microsystems*, Chap. 2:p. 59–62, 2000.

[32] C. S. Rafferty, L. Borucki, and R. W. Dutton. Plastic flow during thermal oxidation of silicon. *Applied Physics Letters*, 54:1516, 1989.

[33] C. S. Rafferty and R. W. Dutton. Plastic analysis of cylinder oxidation. *Applied Physics Letters*, 54:1815, 1989.

[34] S. Bozek, B. Baccus, V. Senez, and Z. Z. Wang. Mesh generation for 3D process simulation and the moving boundary problem. *Simulation of semiconductors devices and processes*, 6:460, 1995.

[35] A. Marmiroli, G. Carnevale, and A. Ghetti. Technology and device modeling in micro and nano-electronics: Current and future challenges. 11:p. 41–54, 2007.

[36] M. E. Law. Process modeling for future technologies. *IBM J. Res. Dev.*, 46:339–346, March 2002.

[37] *TSUPREM-4, SYNOPSYS TCAD.*

[38] V. Senez, D. Collard, P. Ferreira, and B. Baccus. Two-dimensional simulation of local oxidation of silicon: calibrated viscoelastic flow analysis. *IEEE Transactions on Electron Devices*, 43:720–731, May 1996.

[39] R. H. Doremus. Oxidation of silicon: strain and linear kinetics. *Thin Solid Films*, 122:191–196, 1984.

[40] G. Hetherington, K. H. Jack, and J. C. Kennedy. The viscosity of vitreous silica. *Phys. Chem. Glasses*, 5:130, 1964.

[41] T. Uchida and K. Nishi. Formulation of a viscoelastic stress problem using analytical integration and its application to viscoelastic oxidation simulation. *Jpn. J. Appl. Phys.*, 40:p. 6711–6719, 2001.

[42] P.-F. Fazzini, C. Bonafos, A. Claverie, A. Hubert, T. Ernst, and M. Respaud. Modeling stress retarded self-limiting oxidation of suspended silicon nanowires for the development of silicon nanowire-based nanodevices. *Journal of Applied Physics*, 110:033524, 2011.

[43] C. Krzeminski, X.-L. Han, and G. Larrieu. Understanding of the retarded oxidation effects in silicon nanostructures. *Applied Physics Letters*, 100(25):263111, 2012.

[44] E. A Irene, H. Z. Massoud, and E. Tierney. Silicon oxidation studies: Silicon orientation effects on thermal oxidation. *J. Electrochem. Soc.*, 133(6):1253, 1986.

[45] J. L. Ngau, P. B. Griffin, and J. D. Plummer. Silicon orientation effects in the initial regime of wet oxidation. *Journal of The Electrochemical Society*, 149(8):F98–F101, 2002.

[46] E. Kodeba and E. A. Irene. Intrinsic sio_2 film stress measurements on thermall oxidized si. *J. Vac. Sci. Technol. B*, 5(1):15, 1987.

[47] E. Kodeba and E. A. Irene. in-situ stress measurements during thermal oxidation of silicon. *J.*

Vac. Sci. Technol. B, 7(2):163, 1989.

[48] T. J Delph. Intrinsic strain in sio_2 thin films. *J. Appl. Phys.*, 83(2):786, 1998.

[49] R. B. Marcus and T. T. Sheng. The oxidation of shaped silicon surfaces. *J. Electrochem. Soc.*, 129(6):1278, 1982.

[50] L. O. Wilson and R. B. Marcus. Oxidation of curved silicon surfaces. *J. Electrochem. Soc.*, 134(2):481, 1987.

[51] P. Sutardja and W. G. Oldham. Modeling of stress effects in silicon oxidation. *IEEE Trans. elect. Devices*, 36:2415, 1989.

[52] A. Poncet. Finite-element simulation of local oxidation of silicon. *IEEE Trans. on Computer-aided Design*, 4(1):41, 1985.

[53] G. Larrieu and X.-L. Han. Vertical nanowire array-based field effect transistors for ultimate scaling. *Nanoscale*, 5:2437–2441, 2013.

[54] V. Schmidt, H. Riel, S. Senz, S. Karg, W. Riess, and U. Gsele. Realization of a silicon nanowire vertical surround-gate field-effect transistor. *Small*, 2(1):85–88, 2006.

[55] C.-W. Sohn, C. Y. Kang, R.-H. Baek, D.-Y. Choi, H. C. Sagong, E.-Y. Jeong, J.-S. Lee, P. Kirsch, R. Jammy, J.C. Lee, and Y.-H. Jeong. Comparative study of geometry-dependent capacitances of planar fets and double-gate finfets: Optimization and process variation. In *VLSI Technology, Systems, and Applications (VLSI-TSA), 2012 International Symposium on*, pages 1 –2, april 2012.

Tables

	$(B/A)_0$ (μm/min)	$E_{(B/A)}$ (eV)	f_{100}	f_{110}	f_{111}
Standard	$2.058\ 10^{04}$	1.17	1	1.676	1.394
Modif.	$2.058\ 10^{04}$	1.17	1	2.25	1.57

Table 1. Prefactors $(B/A)_0$ and activation energies $E_{(B/A)}$ for the Arrhenius expression of the linear rate constant for the Deal and Grove model. Standard TCAD and modified parameters to take into account the orientation influence are given respectively in the first and second lines of the table.

7. Captions

Figure 1. Top-down fabrication process of the different silicon nanostructures investigated in this work for nanobeams, nanowires and nanorings. Serial A : SEM pictures in cross view of HSQ mask (1) nanobeam, (2) nanopillars and (3) nanoring; Serial B(1-3): SEM pictures after mask transfer by etching in Si substrate; Serial C(1-3): SEM pictures after wet oxidation and strepping oxide by HF.

Figure 2. Schematic of the different systems considered in this work. a) describes the planar bulk oxidation system in order to simulate the oxide bulk growth. b) presents the 2D nanobeam oxidation process where FEM simulations have been undertaken in order to predict the complex oxide film shape. (c) presents the cylinder geometry used for the simulation of the nanowire oxidation. An infinite length nanowire is considered.

Figure 3. Influence of substrate orientations for planar wet oxidation at 850°C. The experimental data of Ngau *et al.* performed at a lower temperature (785°C) are also reported in black symbols [45] whereas modelling results are given in dashed lines. (a) presents in dashed lines the simulation results for the standard Deal and Grove model whereas b) highlights the agreement when the standard linear growth rates are adjusted in order to take into account the influence of the enhanced oxidation for [110] in the short time regime. Similar conclusions to the study of Ngau *et al.* are reached.

Figure 4. Experimental oxidation behaviour for convex and concave silicon nanostructures at 850°C (symbols). Comparison of retarded oxidation effects in the convex/concave cases predicted by the analytic approach using the standard activation volume of TCAD tools based on the viscoelastic model [19] (V_d=75 Å^3) and the activation volume used in this work (V_d=45 Å^3) (lines). a) highlights the retardation is well described for convex geometry but clearly overestimated for the concave nanoobjects. b) shows that a proper calibration of the standard activation volume (V_d=45 Å^3) is necessary in order to describe the influence of concave effects.

Figure 5. (a) Oxide thickness as a function of the nanobeam width for two oxidation times (10 min black color) and 20 min (red color)). The open symbols for the thinnest nanobeams indicate a complete oxidation at mid-height with the presence of a embedded silicon nanowire at the top. (b) presents the characteristics of the nanobeam profile with the influence of the convex (resp. concave) corner influence at the top (resp. bottom). (c) Different SEM images showing the influence of the height and oxidation duration on the nanobeam structure after wet oxidation.

Figure 6. (a)/(c) : SEM images and (b)/(d) 2D FEM simulations of 40 nm wide nanobeams (height 220 nm) for 10 min/20 min of wet oxidation. (b) the two dimensional FEM simulation counterpart. (c) and (d) presents the same properties (structure and simulation) but for 20 min of wet oxidation. The lateral strain distribution σ_{xx} is reported. It shows that a significant compressive strain (above 2 GPa) is obtained at the bottom and the top of the nanobeam explaining the limited oxide growth and the oxide embedded NWs at the top for 20 minutes. For figures (c) & (d), the agreement between the simulation and the SEM image and the presence of a SiNW on the top could be emphasised.

Figure 7. (a) Theoretical oxide thickness predicted by process simulation as a function of the nanobeam width for respectively 110 and 240 nm height nanobeams. The simulation confirms the main experimental trend with constant oxide thickness as function of the nanobeam widths. For 20 min of wet oxidation some difference is observed between 110 and 240 nm height nanobeams which can be related to stress effects. (b) presents the lateral stress building with the oxidation time as function of the nanobeam height. The large stress building for the 110 nm height which explains the modest oxide thickness increase between 10 and 20 min and the difference with the 240 nm nanobeam height. (c) The lateral stress σ_{xx} dependence with the nanobeam geometry is relatively constant along nanobeams width, which explains the experimental trend described in 5.(a).

Figure 8. The different SEM images compare the shape for (a) the nanobeam and (b) the nanowire profile. The TEM characterisation in (a) shows that the nanobeam top has a neck shape whereas (b) presents a vertical uniform profile of the nanowire.

Figure 9. (a) The various symbols report the experimental SiNWs diameters evolution with oxidation for starting 43, 73, 93 and 133 nm diameter which compare well with the 1D modelling counterpart. (b) reports the evolution of experimental and theoretical thickness for the same conditions. (c) describes the linear rate for the different SiNWs with in inset the compressive radial stress building which govern the linear rate decrease. (d) reports the parabolic rate constant for the SiNWs and the hydrostatic pressure variation with the oxidation time (in inset).

Figure 10. Experimental improvement of the silicon nanowires aspect ratio by oxidation. (a) The various symbols report the experimental aspect ratio variation with the silicon nanowire diameters (93 nm down to 33 nm) for respectively 10 min. and 20 min. of wet oxidation. The dashed lines correspond to the experimental trend. The retarded oxidation effects are able to increase significantly the initial ratio aspect above 92 % (b) presents the SEM images of silicon nanowires before the oxidation step while (c) and (d) describe the aspect ratio engineering of the oxidised silicon nanowires (scale bar=100nm).

Figure 11. (a) Variation of the anisotropic aspect ratio for the different SiNWs estimated by the 1D plastic model. The model underestimates the experimental increase in the aspect ratio presented in figure 10. The effect of the retarded oxidation is beneficial for the thinnest SiNWs as observed experimentally. (b) Comparison between the anisotropic character evolution for a configuration where a 43 nm diameter nanowire with no initial oxide and a theoretical configuration where a large initial silicon oxide exceeding the silicon core would be present. (c) The variations with oxidation are reported as a function of the initial anisotropic character.

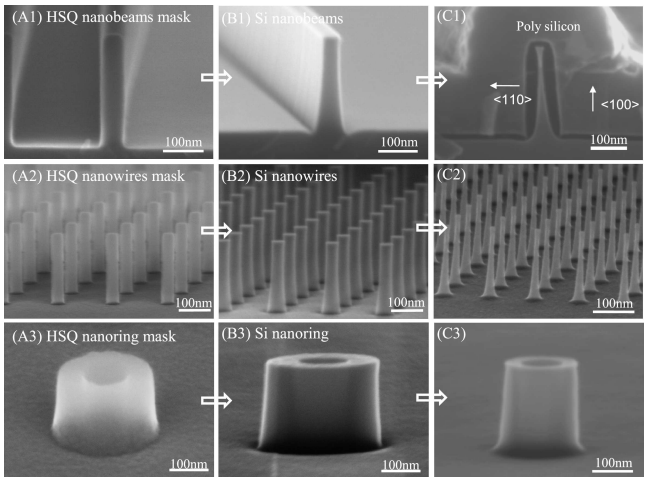
(A1) HSQ nanobeams mask
100nm
(B1) Si nanobeams
100nm
(C1)
Poly silicon
<110>
<100>
100nm
(A2) HSQ nanowires mask
100nm
(B2) Si nanowires
100nm
(C2)
100nm
(A3) HSQ nanoring mask
100nm
(B3) Si nanoring
100nm
(C3)
100nm

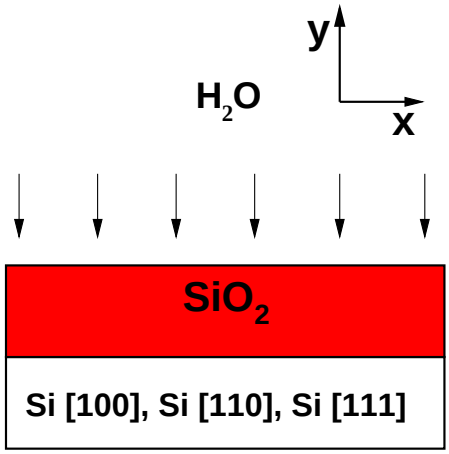

Planar bulk oxidation

(a)

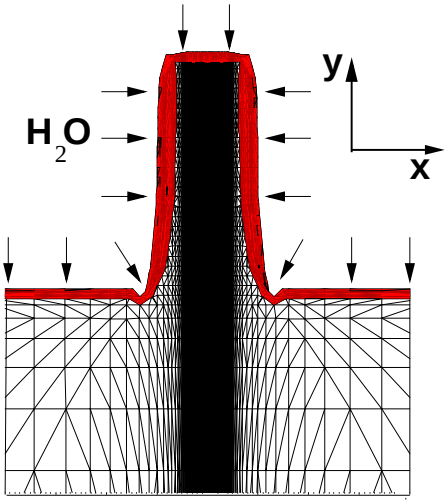

Nanobeam oxidation

(b)

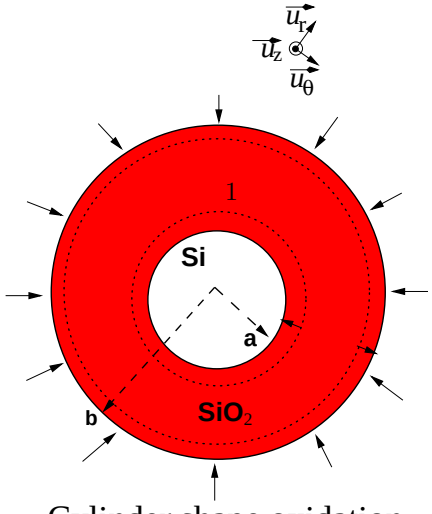

Cylinder shape oxidation

(c)

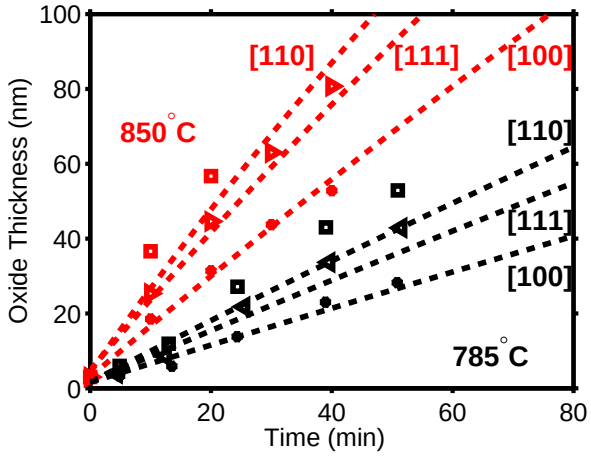
Oxide Thickness (nm)
Time (min)
[110]
[111]
[100]
850°C
[110]
[111]
[100]
785°C
0
20
40
60
80
100

(a)

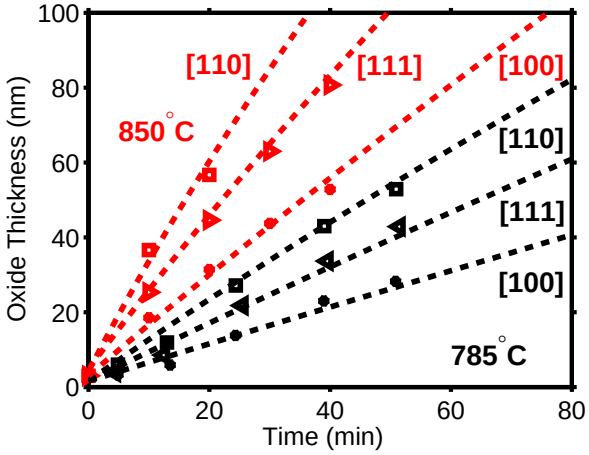
Oxide Thickness (nm)
Time (min)
[110]
[111]
[100]
850°C
[110]
[111]
[100]
785°C
0
20
40
60
80
100

(b)

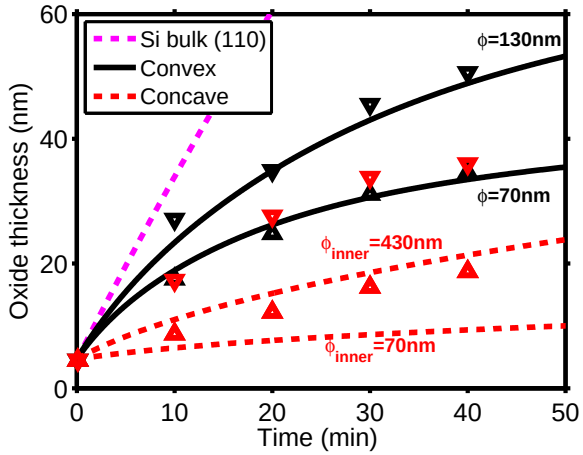
Si bulk (110)
Convex
Concave
ϕ=130nm
ϕ=70nm
ϕinner=430nm
ϕinner=70nm
Oxide thickness (nm)
Time (min)
0
20
40
60
0
10
20
30
40
50

(a)

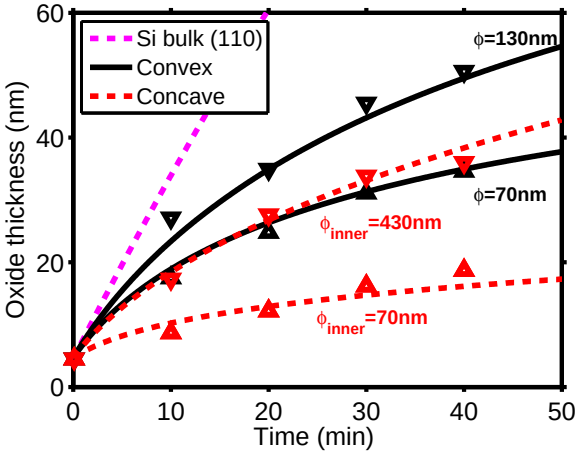
Si bulk (110)
Convex
Concave
ϕ=130nm
ϕ=70nm
ϕinner=430nm
ϕinner=70nm
Oxide thickness (nm)
Time (min)
0
20
40
60
0
10
20
30
40
50

(b)

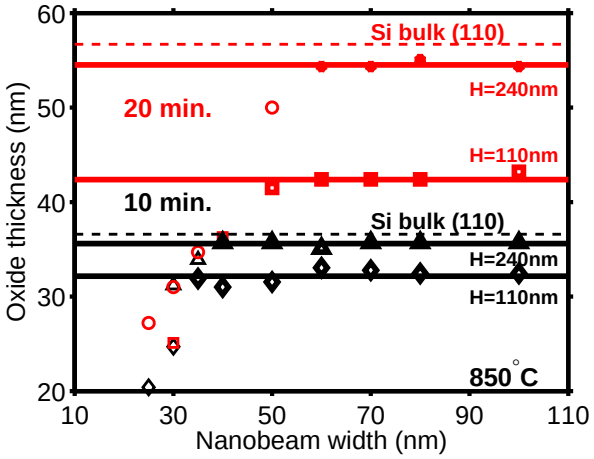
Oxide thickness (nm)
Nanobeam width (nm)
Si bulk (110)
H=240nm
H=110nm
20 min.
10 min.
Si bulk (110)
H=240nm
H=110nm
850 °C
60
50
40
30
20
10
30
50
70
90
110

(a)

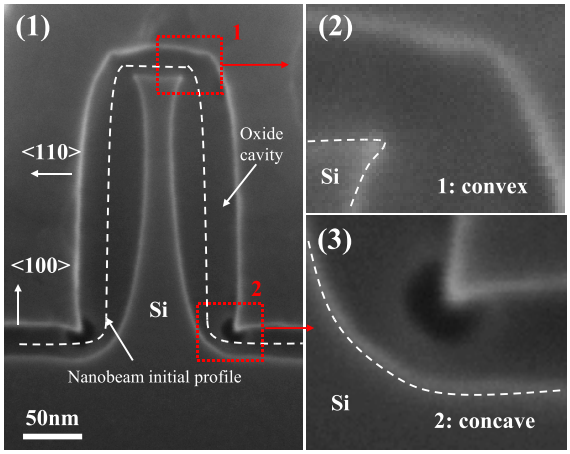
(1)
(2)
(3)
<110>
<100>
Oxide cavity
Si
Nanobeam initial profile
50nm
1: convex
2: concave

(b)

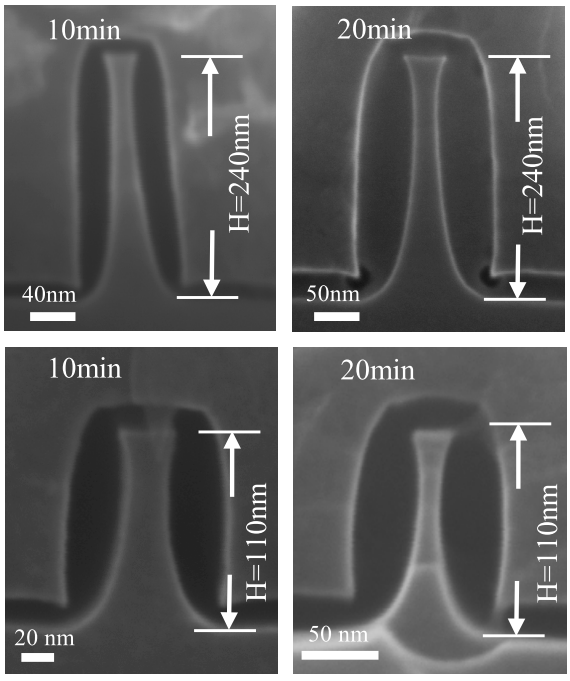
10min
20min
H=240nm
40nm
50nm
10min
20min
H=110nm
20 nm
50 nm

(c)

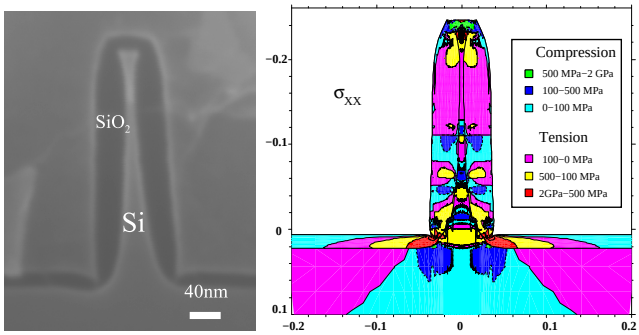
SiO2
Si
40nm
σXX
Compression
500 MPa−2 GPa
100−500 MPa
0−100 MPa
Tension
100−0 MPa
500−100 MPa
2GPa−500 MPa
−0.2
−0.1
0
0.1
0.2

(a) (b)

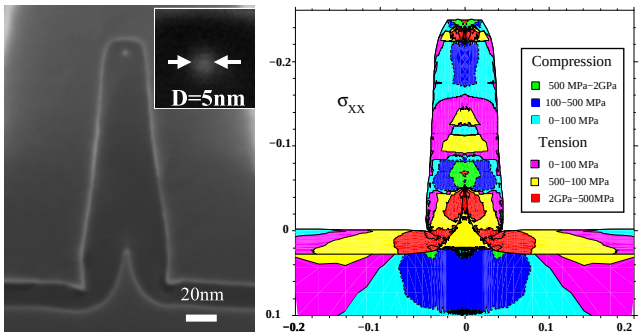
D=5nm
20nm
σXX
Compression
500 MPa−2GPa
100−500 MPa
0−100 MPa
Tension
0−100 MPa
500−100 MPa
2GPa−500MPa
−0.2
−0.1
0
0.1
0.2

(c) (d)

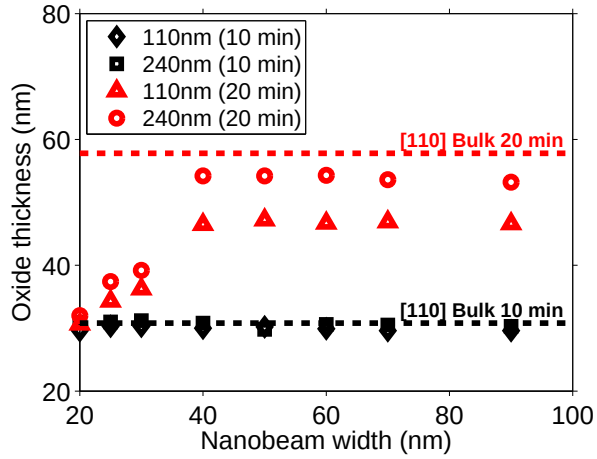
110nm (10 min)
240nm (10 min)
110nm (20 min)
240nm (20 min)
[110] Bulk 20 min
[110] Bulk 10 min
Oxide thickness (nm)
Nanobeam width (nm)
80
60
40
20
20
40
60
80
100

(a)

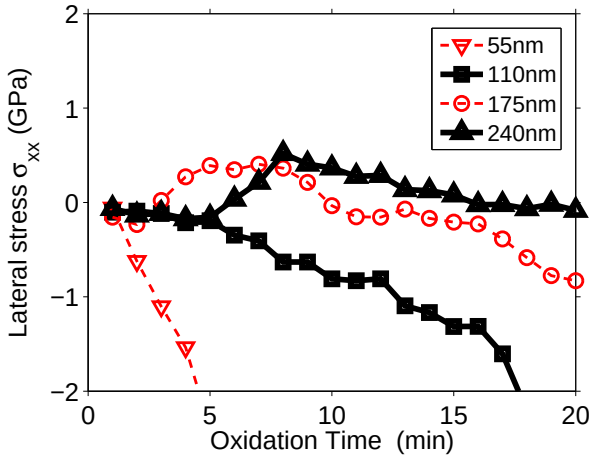
55nm
110nm
175nm
240nm
Lateral stress σxx (GPa)
Oxidation Time (min)
2
1
0
−1
−2
0
5
10
15
20

(b)

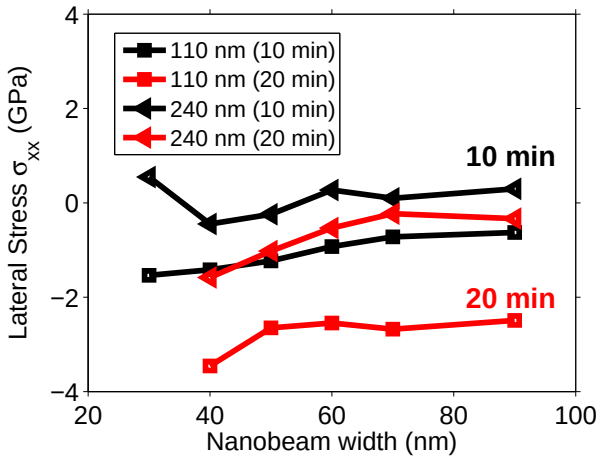
110 nm (10 min)
110 nm (20 min)
240 nm (10 min)
240 nm (20 min)
10 min
20 min
Lateral Stress σxx (GPa)
Nanobeam width (nm)
4
2
0
−2
−4
20
40
60
80
100

(c)

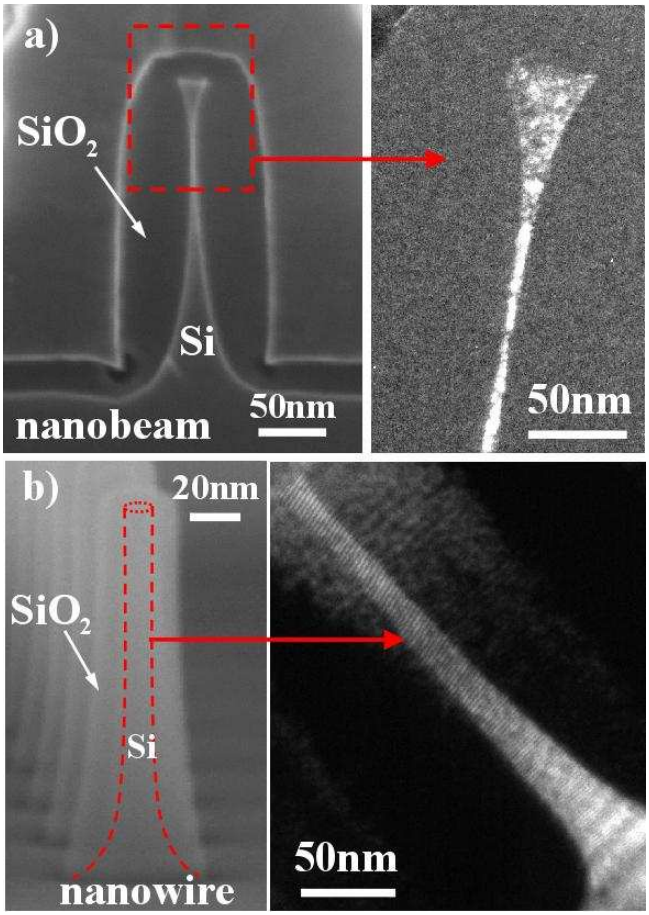
a)
SiO2
Si
nanobeam
50nm
50nm
b)
20nm
SiO2
Si
nanowire
50nm

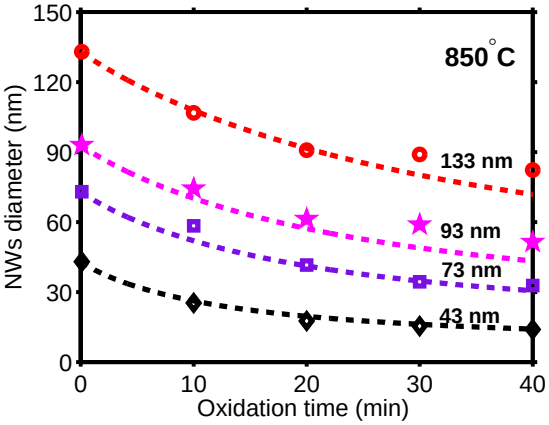
850 °C
133 nm
93 nm
73 nm
43 nm
NWs diameter (nm)
Oxidation time (min)

(a)

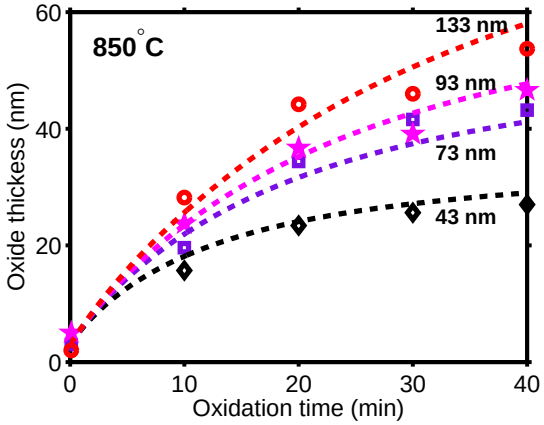
850 °C
133 nm
93 nm
73 nm
43 nm
Oxide thickess (nm)
Oxidation time (min)

(b)

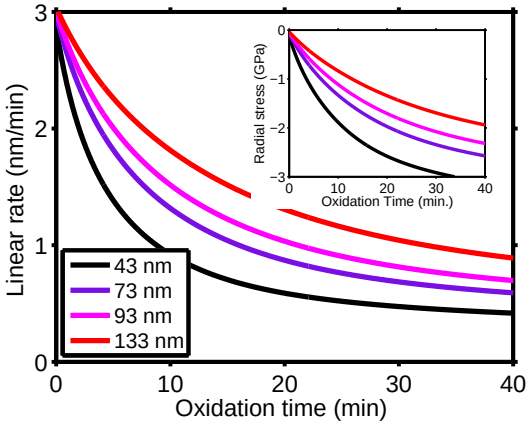
43 nm
73 nm
93 nm
133 nm
Linear rate (nm/min)
Oxidation time (min)
Radial stress (GPa)
Oxidation Time (min.)

(c)

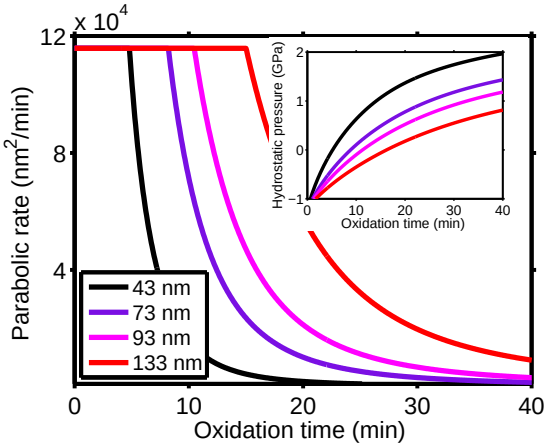
x 10^4
43 nm
73 nm
93 nm
133 nm
Parabolic rate (nm^2/min)
Oxidation time (min)
Hydrostatic pressure (GPa)
Oxidation time (min)

(d)

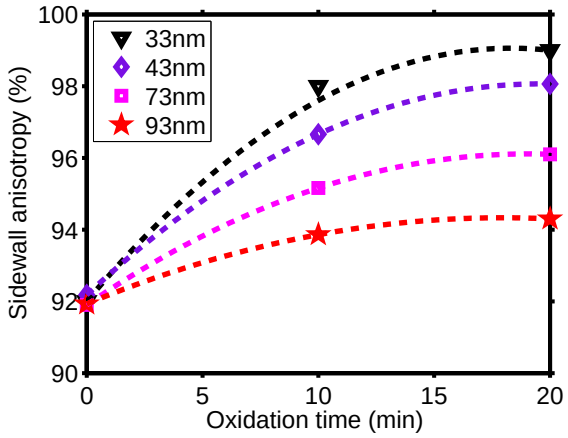
100
98
96
94
92
90
0
5
10
15
20
Sidewall anisotropy (%)
Oxidation time (min)
33nm
43nm
73nm
93nm

(a)

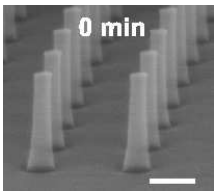
0 min

(b)

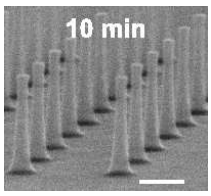
10 min

(c)

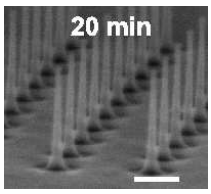
20 min

(d)

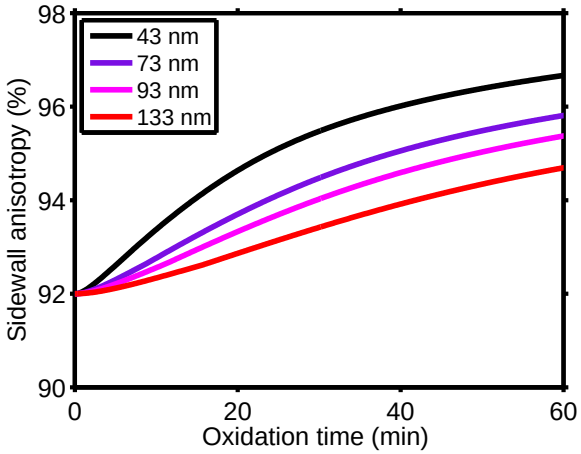
43 nm
73 nm
93 nm
133 nm
Sidewall anisotropy (%)
Oxidation time (min)
98
96
94
92
90
0
20
40
60

(a)

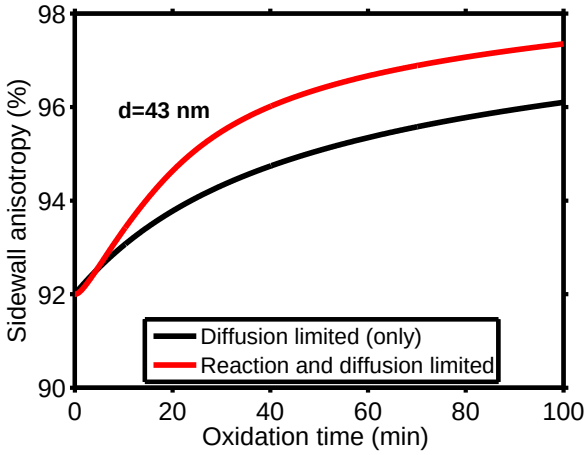
d=43 nm
Diffusion limited (only)
Reaction and diffusion limited
Sidewall anisotropy (%)
Oxidation time (min)
98
96
94
92
90
0
20
40
60
80
100

(b)

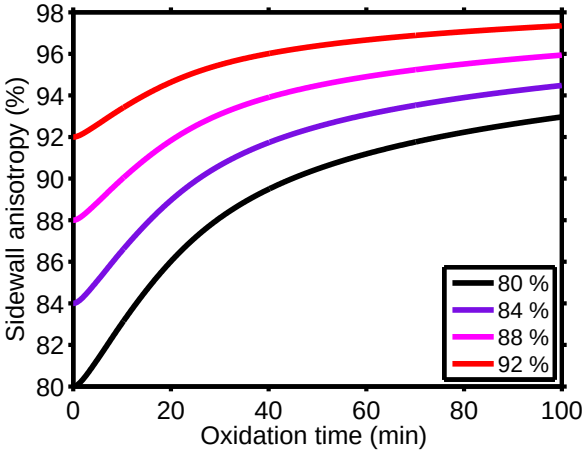
80 %
84 %
88 %
92 %
Sidewall anisotropy (%)
Oxidation time (min)
98
96
94
92
90
88
86
84
82
80
0
20
40
60
80
100

(c)